Journal of Materials Chemistry C

PAPER

View Article Online
View Journal | View Issue

Cite this: J. Mater. Chem. C, 2014, 2, 496

Red emitting Y_2O_3:Eu^{3+} nanophosphors with >80% down conversion efficiency†

A. P. Jadhav,[ab] A. U. Pawar,[a] U. Pal[c] and Y. S. Kang*[a]

Received 3rd October 2013
Accepted 22nd October 2013

DOI: 10.1039/c3tc31939c

www.rsc.org/MaterialsC

Obtaining nanophosphors of a controlled size and shape with a high quantum efficiency is the current challenge for display and imaging technologies. Although the surface state induced luminescence quenching in nanophosphors may be compensated to some extent by incorporating activators like rare-earth ions, or by exploiting their quantum size effect, obtaining nanophosphors with quantum efficiencies as high as their bulk counterparts remains elusive. In the present article, we report on the synthesis of uniform Eu-doped Y_2O_3 nanoparticles, with an average size of 20–53 nm and a down conversion efficiency as high as 85%, using a simple chemical precipitation technique. Along with size control, the effects of Eu^{3+} content on their emission behaviors have been discussed. We believe the low-cost synthesis process of these nanoparticles will greatly enhance their application potential in optical display and bio-imaging technologies.

A Introduction

Transition-metal oxides are well known high luminescent emitters in the visible spectral region.[1,2] High thermal and chemical stabilities, optical transparency in infra-red, and biocompatibility make these materials suitable for applications in flat panel displays, optical amplifiers, and for bio labelling.[3,4] For practical applications, nanostructures of these materials are preferred to their micrometric or sub-micrometric counterparts, as they offer higher spatial resolution in optical devices such as displays, immunoassays, and for DNA assay labelling.[5,6] Frequently, rare earth (RE) ions such as Eu^{3+}, Tb^{3+} and Yb^{3+} are incorporated into these nanostructures to enhance their emission efficiency by exploiting their inter-band transitions which are induced by photo-generated charge carriers (electrons and holes) in the metal-oxide host lattice; *i.e.* through the energy transfer between the RE ions and the host lattice. Apart from the high stability of the rare-earth ions in the metal-oxide matrices, they also improve the emission efficiency of the metal oxides.[7] However, in the nanostructure form, the emission efficiency of metal-oxide phosphors is reduced drastically. This reduction has been associated with several factors including their size, synthesis temperature, crystallinity and their site-selective incorporation of dopant ions.[8–10] While the variations in emission efficiency with each of these parameters have been studied by several research groups, the outcome has remained controversial.[11–13] Nevertheless, in most cases, the emission efficiencies of the rare-earth doped transition-metal oxide nanophosphors appear to be much lower than their bulk counterparts, and the development of nanophosphors with a high quantum efficiency (QE) remains a big challenge.

In the present article, we report on the synthesis of monodispersed Eu-doped Y_2O_3 nanophosphors with a spherical morphology and an emission efficiency as high as 85%, using a simple chemical co-precipitation technique. The contributions of synthesis temperature in controlling the concentration and site selective incorporation of Eu^{3+} in the Y_2O_3 lattice have been studied.

B Experimental

Materials

Yttrium(III) chloride hexahydrate ($YCl_3 \cdot 6H_2O$, 99.9%, Sigma Aldrich), europium(III) chloride hexahydrate ($EuCl_3 \cdot 6H_2O$, Tokyo Chemical Industry Co. Ltd.), sodium carbonate (Na_2CO_3, Junsei Chemicals Co. Ltd.), sodium chloride (NaCl, Duksan Pure Chemicals Co. Ltd.) and oleic acid ($C_{18}H_{34}O_2$, Junsei Chemicals Co. Ltd) have been used as received without further purification.

Synthesis

The nanoparticles of Y_2O_3:Eu^{3+} were synthesized by a chemical co-precipitation technique which utilizes oleic acid as a surfactant and NaCl as a neutral electrolyte.[14] To study the effects of synthesis temperature on the size and optical

[a]Department of Chemistry, Sogang University, 1, Shinsu-dong, Mapo-gu, Seoul, 121-742, Republic of Korea. E-mail: yskang@sogang.ac.kr; Fax: +82 2 701 0967; Tel: +82 2 705 8882

[b]Center for Materials Architecturing, Korea Institute of Science and Technology, Hwarangno 14-gil 5, Seongbuk-gu, Seoul, 136-791, Republic of Korea

[c]Instituto de Fisica, Benemerita, Universidad, Autonoma de Puebla, Apodo, Postal J-48, Puebla, Mexico. Tel: +52 222 2295500 (2047)

† Electronic supplementary information (ESI) available. See DOI: 10.1039/c3tc31939c

properties of the europium doped Y_2O_3 nanoparticles, the reactions were carried out by varying the synthesis temperature between 25 and 100 °C. The pH of the reaction solutions was adjusted to 7 at the respective reaction temperatures. For the reactions at higher temperatures, we used a condenser assembly to maintain a constant reaction temperature throughout the synthesis process. After cooling the solution to room temperature, the precipitate was separated by centrifuging (10 000 rpm, 10 min at 23 °C), washed several times with deionized water, and dried at 120 °C for 6 h in air. The dried samples were then air annealed at 800 °C for 1 h in a muffle furnace.

Characterizations

Structural and morphological analyses of the samples were performed using a Rigaku X-ray diffractometer (Cu Kα, λ = 1.54056 Å) and a JEOL, JEM-2100F transmission electron microscope operating at 200 keV, respectively. The samples for observation were prepared by dispersing a small amount of each sample in cyclohexane, spreading a drop of them over carbon coated copper grids and then drying them under a UV lamp. The surface composition and chemical state of the constituting elements of the samples were studied using a Thermo VG Scientific (England), Multitab 2000 X-ray photoelectron spectrometer. The diffuse reflectance of the samples was studied using a JASCO V660 spectrophotometer. Room temperature photoluminescence (PL) emission of the powder samples was measured using a Hitachi F-7000 fluorescence spectrophotometer equipped with a φ 60 integrating sphere, and the 265 nm emission of a xenon lamp was used as the excitation source.

C Results and discussion

Crystalline Y_2O_3 has a cubic bixbyite structure with an *Ia*3 space group,[15,16] containing 16 formula units in each primitive cell. Of the 32 six-fold coordinated cations in its primitive cell, 8 are centrosymmetric with C_{3i} symmetry and 24 are non-centrosymmetric with C_2 symmetry (Fig. 1).[17] The point symmetry S_6, C_{3i} has an inversion center and a smaller crystal field, which doesn't allow for electron–dipole transitions in the absence of lattice distortion (either thermal or due to impurity incorporation). The C_2 sites however, are non-centrosymmetric *i.e.* they have no center of inversion, allowing for electron–dipole transitions, and therefore, they are predominantly responsible for the luminescent emissions when occupied by transition metal ions.[18–20] The cubic phase of yttrium oxide shows the presence of Y^{3+} in two different environments (C_2 or S_6) surrounded by six oxygen atoms. The isomorphic substitution of europium ions in the Y_2O_3 will usually occupy these symmetry sites (low symmetry C_2 and high symmetry S_6) to form energy level structures as represented in Fig. 1. The number of C_2 sites is about three times higher than the number of S_6 sites in the Y_2O_3 crystal. Ranson *et al.* and Buijs *et al.* have shown the existence of different energy transfer channels between the Eu^{3+} ions occupying different crystallographic sites in the yttrium oxide. Among these energy transfer channels the path length of channel (3) is long enough to affect the fluorescent evolution of $^5D_0$ (C_2).[21,22] The presence of Eu^{3+} ions at the S_6 site mostly results in a slower emission due to the lower probability of electronic transition from that site.[23,24] The generation of non-radiative relaxations can result in the lowering of the total emission efficiency. Due to the same reason, when doped with Eu, most of the incorporated Eu^{3+} ions occupy the C_2 sites of the Y_2O_3 lattice, favoring the $^5D_0 \rightarrow {}^7F_2$ interband transitions. However, when incorporating the ions at a higher concentration, a part of the Eu^{3+} ions can occupy the C_{3i} sites, causing a reduction in the luminescence efficiency.[25]

Incorporation of rare earth dopant ions into the Y_2O_3 nanostructures strongly depends on their synthesis temperature; a higher synthesis temperature aids incorporation. Fig. 2 shows that the synthesized Y_2O_3:Eu^{3+} nanoparticles have a quasi-spherical morphology with a smooth surface and that their average size increases with synthesis temperature. A higher synthesis temperature also helps to form perfect crystalline structures of the cubic phase of the Y_2O_3; this can be observed from the X-ray diffraction (XRD) patterns of the heat treated Y_2O_3:Eu^{3+} nanophosphors (Fig. 3).

Fig. 3 shows the XRD patterns of the Y_2O_3:Eu^{3+} samples prepared at different reaction temperatures and air-annealed at 800 °C for 1 h. All the samples revealed well resolved diffraction peaks corresponding to the body centered cubic structure (space group *Ia*3) of Y_2O_3 (JCPDS # 83-0927). Although there was no noticeable change in the peak positions, the intensity of the most prominent peak (222) increased slightly up to 75 °C, and then decreased. The (321) peak which appeared in the sample prepared at 25 °C, disappeared for the samples prepared at higher temperatures. The disappearance of this peak is probably associated with the reorientation of the crystal planes in the nanocrystals. The absence of any additional peaks related to Eu, or its oxide, in the XRD spectra of the samples indicates effective incorporation of the activator into the host lattice. The lattice constant '*a*' of the samples was calculated using the equation $1/d^2 = (h^2 + k^2 + l^2)/a^2$, and the resulting values of 10.614 ± 0.002 Å and 10.614 ± 0.001 Å, for the samples prepared at 25 °C and at higher temperatures (50–100 °C), respectively, were very close to the standard value for the cubic bixbyite Y_2O_3 (a = 10.608 Å; JCPDS 83-0927). The average grain sizes of the Y_2O_3:Eu^{3+} samples synthesized at different reaction temperatures were calculated using the Scherrer formula and presented in Table 1. It can be noted that, neither the diffraction peaks (Fig. 3) nor the average grain size vary in a regular manner with the increase in synthesis temperature. On increasing the synthesis temperature, the Eu^{3+} ions of a higher quantity can be incorporated into the nanoparticles (Table 1), resulting in a decrease in their room temperature PL emissions (Fig. 4).

Table 1 presents the data obtained from X-ray photoelectron spectroscopy (XPS), XRD, TEM and QE measurements. It was observed that by increasing the reaction temperature, a higher amount of Eu^{3+} ions could be incorporated into the Y_2O_3 nanoparticles, (see Table 1 and ESI†) without hindering their growth and crystallinity. However, their room temperature PL emissions decreased with the increase in synthesis temperature (Fig. 4).

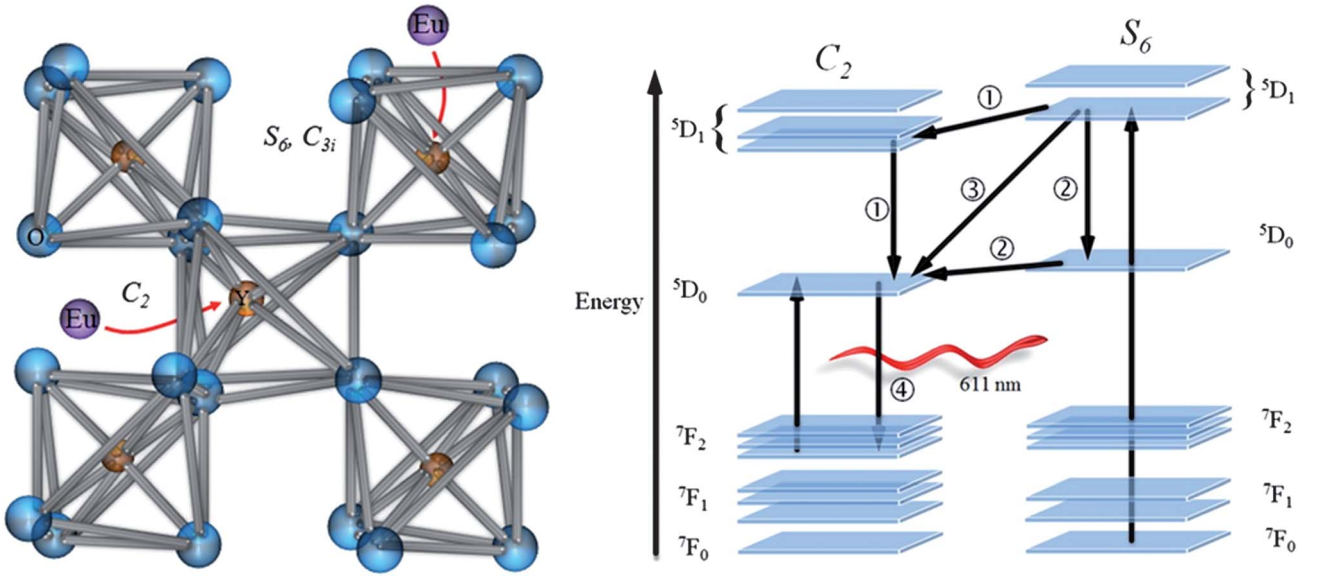

Fig. 1 The cubic bixbyite structure of Y_2O_3 with both C_2 and C_{3i} symmetry sites and $^5D_0 \rightarrow {}^7F_J$ ($J = 0$, 1, 2) transitions in the Y_2O_3:Eu^{3+}.

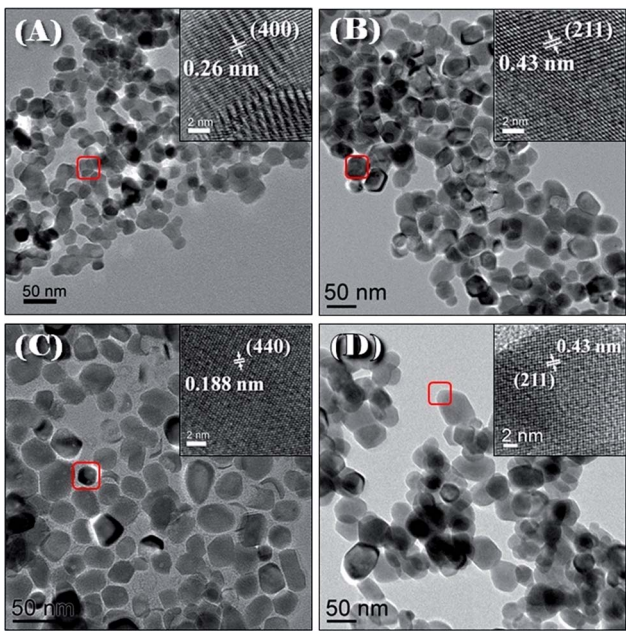

Fig. 2 Typical transmission electron microscopy (TEM) images of the Y_2O_3:Eu^{3+} nanoparticles synthesized at (A) 25, (B) 50, (C) 75, and (D) 100 °C after annealing at 800 °C for 1 h. The insets represent the respective HRTEM images, with the lattice plane matching the diffraction pattern of Y_2O_3.

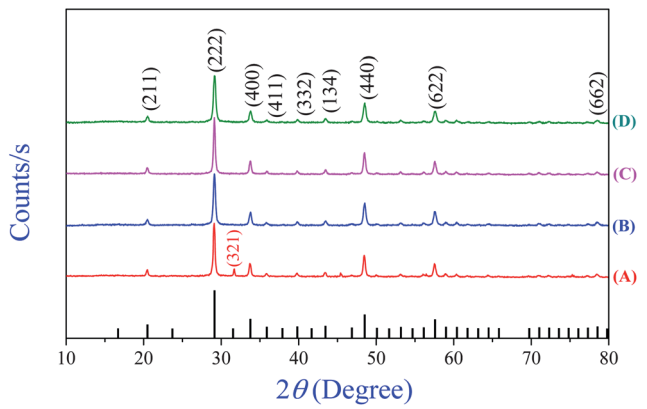

Fig. 3 XRD patterns of Y_2O_3:Eu^{3+} nanoparticles synthesized at (A) 25, (B) 50, (C) 75 and (D) 100 °C after calcination treatment at 800 °C for 1 h. The XRD patterns were compared with a standard JCPDS card (83-0927) of yttrium oxide.

Table 1 Surface composition, particle size, and PL estimated QE values of Y_2O_3:Eu^{3+} nanoparticles synthesized at different reaction temperatures

Reaction temperature °C	XPS composition (atom %)			Ave. particle/crystallite size (nm)		
	Y	O	Eu	TEM	XRD	%QE
25	15.52	84.15	0.23	28.53	25.50	85.49
50	35.38	63.14	1.47	39.50	23.50	36.92
75	36.36	62.16	1.48	51.00	28.50	27.66
100	36.56	61.87	1.58	53.00	21.00	24.40

The room temperature PL spectra of all the samples revealed the characteristic emission bands associated with Eu^{3+} ions, *i.e.* the $^5D_0 \rightarrow {}^7F_J$ ($J = 0$, 1, 2) interband transitions associated with the spin forbidden f–f transition (Fig. 4). The prominent emission at 612 nm is associated with the $^5D_0 \rightarrow {}^7F_2$ transition and the relatively weak emissions at around 581.6 nm are due to the $^5D_0 \rightarrow {}^7F_0$ transition. While the weaker emissions which appear at around 587.8, 593.4 and 599.6 nm correspond to the $^5D_0 \rightarrow {}^7F_1$ transitions, the emission at around 631.2 nm corresponds to the $^5D_0 \rightarrow {}^7F_2$ transition. The $^5D_0 \rightarrow {}^7F_1$ transition is known as the parity allowed magnetic dipole transition ($\Delta J = 1$) and its intensity usually remains independent of the host crystal. In the case of the $^5D_0 \rightarrow {}^7F_1$ electric dipole

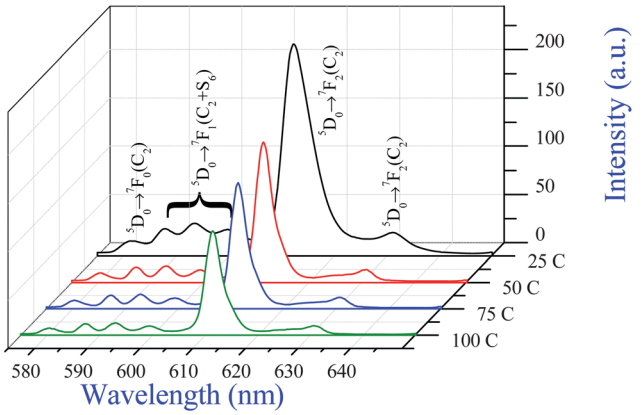

Fig. 4 Room temperature PL spectra of the Y_2O_3:Eu^{3+} nanoparticles synthesized at 25, 50, 75 and 100 °C. All the samples were air annealed at 800 °C for 1 h. The 265 nm emission of a xenon lamp was used for the excitation.

transition ($\Delta J = 2$) which is highly affected by the local environment around Eu^{3+}, the emission intensity depends on the symmetry of the crystal field around the europium ions.[26] The nanoparticles synthesized at RT manifest the highest emission intensity. The emission intensity of the nanoparticles reduced to about 41, 36 and 23% when they were synthesized at 50, 75 and 100 °C, respectively. Incorporation of Eu^{3+} ions in higher concentrations (for the samples synthesized at higher temperatures) generated nonradiative defect centers (killer or quencher ions) in the host lattice, quenching their luminescent emissions either through the loss of energy due to cross-relaxation, excitation migration between the activators (Eu^{3+}), or through the enhanced nonradiative recombination of the photo-generated charge carriers (electrons and holes). On the other hand, the XPS results presented in Table 1 indicate that apart from a lower % of Eu^{3+} ions, the sample synthesized at RT (25 °C) contains high Y vacancy sites in its crystalline lattice, which favors Eu^{3+} ion incorporation at the non-centrosymmetric C_2 sites.

Considering the % reflectance of the powder samples at an excitation wavelength of 265 nm, the QE of the nanophosphors was calculated as:

$$\%\mathrm{QE} = \frac{\text{Number of emitted photons}}{\text{Number of excited photons}} \times 100$$

where the number of emitted photons is considered to be proportional to the integrated intensity of the PL emission, and the number of absorbed photons is considered to be proportional to the intensity of the excitation radiation (after reflectance correction). For the estimation of QEs, the excitation and emission intensities for each sample were measured carefully at least 3 times using a commercial Hitachi F-7000 fluorescence spectrophotometer equipped with a φ 60 integrating sphere. From Table 1, we can see that the estimated QE value decreases gradually with an increase in synthesis temperature. However, the nanophosphors synthesized at RT revealed a QE of about 85%, which is much greater than the reported QE value (~78%) for pure Y_2O_3:Eu^{3+} at the nanometer size range.[27]

Apart from the Eu^{3+} concentration, the QE of the Y_2O_3:Eu^{3+} nanophosphor also appears to be strongly dependent on the particle size and crystallinity of the nanophosphor. Goldburt *et al.* have reported an increase of the QE value for the Y_2O_3:Tb^{3+} nanophosphors when their particle size decreased from 10 to 4 nm, obeying an inverse proportional relationship to the square of the particle size.[28] However, Dijken *et al.* have reported an opposite trend.[29] In fact, reports on the QE values of the Y_2O_3:Eu^{3+} nanocrystals have been inconsistent, which is mainly due to the differences in the synthesis techniques used. Nanocrystals synthesized by different methods manifest different structures, morphologies, and surface characteristics. Schmechel *et al.* have reported that the QE of $^5D_0$ emissions in a commercial bulk Y_2O_3:Eu^{3+} sample (92%), with an average grain size of about 5 μm, reduces to less than 10% when the grain size reduces to between 5–10 nm.[30] A reduction in the QE value by about 30% has also been reported by Dhanraj *et al.* for their sol–gel thermolysis grown nanocrystals.[31] In contrast, Wakefield *et al.* have reported an increase in QE for their Y_2O_3:Eu^{3+} nanocrystals with a size range of 70–100 nm.[32] However, their estimated QE value for commercial bulk Y_2O_3:Eu^{3+} was far below that of the QE values reported by other authors.[33]

The reduction of PL intensity for our Y_2O_3:Eu^{3+} nanoparticles synthesized at higher reaction temperatures is mainly due to the increase in the Eu : Y ratio (see Table 1). As mentioned earlier, there are only two possible sites for the Eu^{3+} ions to occupy in the Y_2O_3 lattice, *i.e.* either at the centrosymmetric C_{3i} sites or at the non-centrosymmetric C_2 sites.[20] Although the Eu^{3+} ions can occupy both the lattice and the interstitial sites of the crystalline host, due to the similar ionic radius of Y and Eu (104 and 108.7 pm, respectively) most of the Eu^{3+} ions are able to occupy the lattice sites and replace the Y ions without affecting the lattice parameter of the host considerably, as we can see from their HRTEM images (see Fig. 2). However, for the incorporation of the Eu^{3+} dopant at a high concentration, after filing up the limited C_2 sites available they are either incorporated at the centrosymmetric C_{3i} sites or at the interstitial sites, where they behave as luminescence quenching centers in the Y_2O_3 particles and facilitate the transfer of energy from radiative centers to nonradiative centers. From Table 1, we can see that the nanoparticles synthesized at RT are highly luminescent, with QE values as high as 85%. The QE value of the nanoparticles reduces to about 37, 27 and 24% for reaction temperatures of 50, 75 and 100 °C, respectively.

Taking into account all the aspects discussed above, this report indicates that the higher PL emission in the samples synthesized at RT can be attributed to its high yttrium (Y) vacancy centres, which favour the incorporation of Eu^{3+} ions at the lattice sites. While the smooth non-faceted surface reduces surface scattering (due to a lower diffuse reflectance), the high Y vacancy sites in the nanocrystals synthesized at RT facilitate the accommodation of dopant ions and therefore enhance the transfer of the absorbed energy to the Eu^{3+} ions.[34,35] On the other hand, high temperature thermal annealing helps to eliminate undesired contaminants from the particle surface. It must be noted (from XPS spectra of the samples shown in

Fig. S1 of ESI†) that the sample synthesized at RT has the lowest carbon content.

D Conclusions

Using a simple chemical co-precipitation technique, Y_2O_3:Eu^{3+} nanoparticles with an average size of 13–28 nm and a down conversion efficiency as high as 85% were synthesized. A highly Y deficient Y_2O_3 crystal lattice accommodates Eu^{3+} ions well at the vacancy sites even at a concentration as low as 0.23 atom%, resulting in drastically enhanced emission efficiency. While a higher synthesis temperature helps to grow larger nanoparticles with a higher Eu^{3+} ion content, higher radiation scattering from their faceted surface and the positioning of the incorporated Eu^{3+} ions at the electric–dipole transition prohibited C_{3i} sites, reduces their emission efficiency. The well dispersed nanophosphors of uniform size which are synthesized at room temperature using this simple and low-cost process may be very attractive for applications in display technologies.

Acknowledgements

This work was financially supported by Energy Technology Research and Development 2008 and the Brain Korea 21.

Notes and references

1 L. Irimpan, V. P. N. Nampoori, P. Radhakrishnan, A. Deepthy and B. Krishnan, *J. Appl. Phys.*, 2007, **102**, 063524.
2 C. Y. Wang, C. Y. Liu, Y. Wang and T. Shen, *J. Colloid Interface Sci.*, 1998, **197**, 126–132.
3 G. Liu and X. Chen, in *Handbook on the Physics and Chemistry of Rare Earths Optical Spectroscopy*, ed. K. A. Gschneidner, Jr, J. C. G. Bünzli and V. K. Pecharsky, N. Holland, 2007, vol. 37, p. 132.
4 G. Blasse and B. C. Grabmaier, in *Luminescent Materials*, Springer, Berlin, Heidelberg, Germany, 1994.
5 P. K. Sharma, R. K. Dutta and A. C. Pandey, *J. Nanopart. Res.*, 2012, **14**, 731.
6 T. Hirai and T. Orikoshi, *J. Colloid Interface Sci.*, 2004, **69**, 103.
7 W. R. Liu, C. H. Huang, C. P. Wu, Y. C. Chiu, Y. T. Yeh and T. M. Chen, *J. Mater. Chem.*, 2011, **21**, 6869.
8 P. D. Rack, J. C. Heikenfeld and A. J. Steckl, in *Handbook of Luminescence, Display Materials and Devices*, ed. H. S. Nalwa and L. S. Rohwer, American Scientific Publishers, Stevenson Ranch, 2003, vol. 3.
9 S. W. Mhin, J. H. Ryu, K. M. Kim, G. S. Park, H. W. Ryu, K. B. Shim, T. Sasaki and N. Koshizaki, *Nanoscale Res. Lett.*, 2009, **4**, 888–895.
10 Z. Chen, Y. W. Yan, J. M. Liu, Y. Yin, H. Wen, G. Liao, C. Wu, J. Zao, D. Liu, H. Tian, C. Zhang and S. Li, *J. Alloys Compd.*, 2009, **478**, 679–683.
11 Q. Li, L. Gao and D. Yan, *Nanostruct. Mater.*, 1997, **8–7**, 825–831.
12 A. Camenzind, R. Strobel, F. Krumeich and S. E. Pratsinis, *Adv. Powder Technol.*, 2007, **18**(1), 5–22.
13 P. K. Sharma, R. Nass and H. Schmidt, *Opt. Mater.*, 1998, **10**, 161–169.
14 A. P. Jadhav, C. W. Kim, H. G. Cha, A. U. Pawar, N. A. Jadhav, U. Pal and Y. S. Kang, *J. Phys. Chem. C*, 2009, **113**, 13600–13604.
15 F. Hanic, M. Hartmova, G. G. Knab, A. A. Uruskovkkaya and K. S. Bagdasarov, *Acta Crystallogr., Sect. B: Struct. Sci.*, 1984, **40**, 76–82.
16 Y. N. Xu, Z. Gu and W. Y. Ching, *Phys. Rev. B: Condens. Matter Mater. Phys.*, 1997, **56**, 14993–15000.
17 A. Gajović, N. Tomašić, I. Djerdj, D. S. Su and K. Furić, *J. Alloys Compd.*, 2008, **456**, 313–319.
18 J. Silver, M. I. Martinez-Rubio, T. G. Ireland and R. Withnall, *J. Phys. Chem. B*, 2001, **105**, 7200–7204.
19 M. Klintenberg, S. Edvardsson and J. O. Thomas, *J. Alloys Compd.*, 1998, **275–277**, 174–176.
20 E. Husson, C. Proust, P. Gillet and J. P. Itie, *Mater. Res. Bull.*, 1999, **34**, 2085–2092.
21 R. M. Ranson, E. Evangelou and C. B. Thomas, *Appl. Phys. Lett.*, 1998, **72**, 2663.
22 M. Buijs, A. Meyerink and G. Blasse, *J. Lumin.*, 1987, **37**, 9.
23 H. Forest and G. Ban, *J. Electrochem. Soc.*, 1969, **116**, 474–478.
24 E. Zych, M. Karbowiak, K. Domagala and S. Hubert, *J. Alloys Compd.*, 2002, **341**, 381–384.
25 A. Kornad, T. Fries, A. Gahn, F. Kummer, U. Herr, R. Tideeks and K. Samwer, *J. Appl. Phys.*, 1999, **86**, 3129.
26 R. Krsmanović, Ž. Antić, M. G. Nikolić, M. Mitrić and M. D. Dramićanin, *Ceram. Int.*, 2011, **37**, 525–531.
27 B. Chen, Q. Meng, H. Zhong, J. Sun, L. Cheng, Y. Peng, T. Yu and M. Chen, *J. Nanosci. Nanotechnol.*, 2008, **72–74**, 1165–1169.
28 E. T. Goldburt, B. Kulkarni, R. N. Bhargava, J. Taylor and M. Libera, *J. Lumin.*, 1997, **72–74**, 190.
29 A. van Dijken, J. Makkinje and A. Meijerink, *J. Lumin.*, 2001, **92**, 323.
30 R. Schmechel, M. Kennedy, H. Von Seggern, H. Winkler, M. Kolbe, R. A. Fischer, X. M. Li, A. Benker, M. Winterer and H. Hahn, *J. Appl. Phys.*, 2001, **89**, 1679.
31 J. Dhanraj, R. Jagannathan, T. R. N. Kutty and C. H. Lu, *J. Phys. Chem. B*, 2001, **105**, 11098–11105.
32 G. Wakefield, E. Holland, P. J. Dobson and J. L. Hutchison, *Adv. Mater.*, 2001, **13**, 1557.
33 R. G. Pappalardo and R. B. Hunt, Jr, *ECS J. Solid State Sci. Technol.*, 1985, **132–3**, 721–730.
34 L. Li, C. K. Tsung, Z. Yang, G. D. Stucky, L. Sun, J. Wang and C. Yan, *Adv. Mater.*, 2008, **20**, 903–908.
35 K. L. Frindell, M. H. Bartl, M. R. Robinson, G. C. Bazan, A. Popitsch and G. D. Stucky, *J. Solid State Chem.*, 2003, **172**, 81–88.

